

Strong margin influence on the Arctic Ocean barium cycle revealed by Pan-Arctic Synthesis

Laura M. Whitmore^{1*}^Δ, Alan M. Shiller^{1*}, Tristan J. Horner², Yang Xiang³, Maureen E. Auro², Dorothea Bauch⁴, Frank Dehairs⁵, Phoebe J. Lam³, Jingxuan Li⁶, Maria T. Maldonado⁶, Chantal Mears⁷, Robert Newton⁸, Angelica Pasqualini⁹, H el ene Planquette¹⁰, Robert Rember¹¹, Helmuth Thomas⁷

¹School of Ocean Science and Engineering, University of Southern Mississippi, Stennis Space Center, Mississippi, USA; ²NIRVANA Laboratories, Woods Hole Oceanographic Institution, Woods Hole, MA 02543, USA; ³Department of Ocean Sciences, University of California, Santa Cruz, CA 95064 USA; ⁴GEOMAR Helmholtz Centre for Ocean Research, Kiel, Germany; ⁵Analytical, Environmental and Geochemistry, Vrije Universiteit Brussel, 1050 Brussels, Belgium; ⁶Earth Ocean & Atmospheric Sciences, University of British Columbia, Vancouver, BC, Canada; ⁷Institute of Carbon Cycles, Helmholtz Centre Hereon, D-21502 Geesthacht, Germany; ⁸Lamont-Doherty Earth Observatory, Columbia University; ⁹Department of Earth and Environmental Engineering, Columbia University, New York, NY, USA; ¹⁰Univ Brest, CNRS, IRD, Ifremer, LEMAR, F-29280 Plouzane, France; ¹¹International Arctic Research Center, University of Alaska Fairbanks, Fairbanks, Alaska 99775, USA

Corresponding author: Laura M. Whitmore (lmwhitmore@alaska.edu) and Alan M. Shiller (alan.shiller@usm.edu)

^ΔCurrent Institution: College of Fisheries and Ocean Sciences, University of Alaska Fairbanks, Fairbanks, AK, USA

Contents of this file

Text S1 to S12

Figures S1 to S11

Tables S1 to S4

Introduction

The information in this supplemental includes additional text, tables, and figures. Presented is an expansion on the methods presented in the manuscript, intercalibration of trace element data, and additional supportive figures toward the discussion in the manuscript. Details can be found in the sections below.

Text S1. Sea Ice Extent during the cruise months

The expeditions all occurred between July and October. These months follow spring melt and reach the sea ice minimum. Active sea ice formation was not a substantial part of the system at the time of sampling. (Figure S1 extracted from the National Snow and Ice Data Center). July sampling occurred in the Labrador Sea (no sea ice coverage) and is not depicted in the following figure.

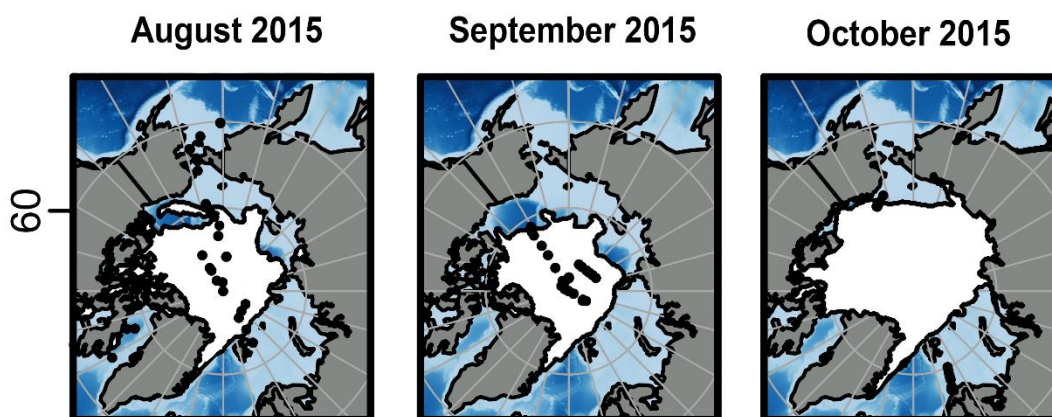


Figure S1. Sea Ice Extent during the 2015 GEOTRACES Expeditions with sampling locations overlain. Image does not convey information about sea ice concentration. Shapefiles from NSIDC (Fetterer et al., 2017).

Text S2. Additional Sampling and Analytical Protocols for dBa

Filtered seawater was collected into acid-washed 125 mL HDPE bottles. Acid washing procedures met GEOTRACES standards (www.geotraces.org/cookbook): bottles were filled with ~10% HCl (Reagent Grade) and soaked overnight at ~60°C (repeated 3 times). Bottles were then rinsed with DI water. Shipboard sampling was conducted by filtration through a 0.45 micron supor filter, each bottle was rinsed with seawater (3x) before collection of the sample.

GN01

At the University of Southern Mississippi (USM) Center for Trace Analysis, dissolved Ba was determined using an ICP-MS (ThermoFisher Element XR) in low resolution; samples were introduced with a PC3 spray chamber (Elemental Scientific). Prior to

analysis, samples were acidified to 0.024 M HCl (Fisher Optima). In preparation for analysis, following isotope dilution methods (Klinkhammer and Chan, 1990), samples were diluted 30-fold with ultra-pure water and spiked with enriched ^{135}Ba solution (Oak Ridge National Laboratory) to a target $^{138/135}\text{Ba}$ ratio between 0.5 and 1. Standards and GEOTRACES reference samples (GS & GD, distributed from the 2008 GEOTRACES Intercalibration Cruise) were analyzed in every run for reproducibility, which was within < 2% RSD (Table S1).

GN02/3

At Vrije Universiteit Brussel (VUB), a volume of 0.25 ml of sample was pipetted into an acid cleaned 15 mL polyethylene tube and acidified with 0.15 ml concentrated ultra-pure nitric acid to ensure the stability of Ba measurements. This acidified sub-sample was spiked with 0.15 ml of a ^{135}Ba -spike solution yielding a $^{138/135}\text{Ba}$ ratio between 0.7 and 1 to minimize error propagation (Klinkenberg et al., 1996; Webster, 1960). Subsequently, the sample was diluted 30-fold with 7 ml Milli-Q grade water to reduce salt content to less than 0.2%. Quantities of sample, spike and dilution water were assessed gravimetrically. The same procedure was employed to prepare blanks (Milli-Q grade water) and reference waters: SLRS-5 & SLRS-3 (National Research Council Canada; Ba concentrations = $14.0 \pm 0.5 \mu\text{g L}^{-1}$ and $13.4 \pm 0.6 \mu\text{g L}^{-1}$, respectively) and 'OMP' seawater (Mediterranean seawater prepared at Observatoire Midi Pyrénées, Toulouse, France; Ba concentration = $10.4 \pm 0.2 \mu\text{g L}^{-1}$). Isotope ratios were measured by sector-field inductively-coupled plasma mass spectrometry (SF-ICP-MS; Element 2, Thermo Finnigan). Reproducibility of our method is within < 2 % (RSD) as tested on repeat preparation of SLRS-5 (Table S1).

GN04

At the University of University of Alaska, Fairbanks, dissolved Ba was determined as done at the University of Southern Mississippi (see above GN01) with the following changes: The samples were diluted 100-fold with ultra-pure water (rather than 30-fold) and analyzed by ICP-MS (ThermoFisher Element 2). Furthermore, sample spikes target a $^{138/135}\text{Ba}$ ratio between 1 and 2. Standards and NRC NASS reference samples (NASS-6 and NASS-7, were analyzed in every run for reproducibility, which was within < 2% RSD (Table S1).

Table S1. Reproducibility and reference standards for dBa and $\delta^{138}\text{Ba}$.

Lab	Parameter	Standard	Referenced value	Measured value	RSD %	n	Detection limit
VUB	dBa	SLRS 5 (ppm)	14.0 +/- 0.5	14.02 +/- 0.21	1.53	15	4.7 nM
VUB	dBa	SLRS 3 (ppm)	13.4 +/- 0.6	13.25 +/- 0.33	2.49	15	7.2 nM
VUB	dBa	OMP (ppm)	10.4 +/- 0.2	10.43 +/- 0.24	2.30	7	5.3 nM
USM	dBa	GS (nmol/kg)		44.3 +/- 0.8	1.80	12	2.4 nmol/kg

USM	dBa	GD (nmol/kg)	54.1 +/- 0.9	1.70	12	2.7 nmol/kg
UAF	dBa	NASS-6 (nM)	48.1 +/- 0.8	1.70	18	1.6 nM
UAF	dBa	NASS-7 (nM)	33.1 +/- 0.7	1.43	14	2.1 nM
WHOI	dBa	GSP (nM)	35.4 +/- 0.8		5	
WHOI	dBa	GSC (nM)	41.8 +/- 0.9		8	
WHOI	dBa	D1 (nM)	101.1 +/- 2.0		13	
WHOI	$\delta^{138}\text{Ba}$	GSP (‰)	0.61 +/- 0.04		5	
WHOI	$\delta^{138}\text{Ba}$	GSC (‰)	0.54 +/- 0.04		8	
WHOI	$\delta^{138}\text{Ba}$	D1 (‰)	0.33 +/- 0.03		13	

Text S3. Additional Analytical Protocols for dissolved $\delta^{138}\text{Ba}$ (GN01)

Sample solutions were aspirated at 140 $\mu\text{L}/\text{min}$ with ~ 1 L/min Ar through a PFA micro-concentric nebulizer (Elemental Scientific) and desolvated in an Aridus II (CETAC). The resultant aerosol was introduced into the MC-ICP-MS and admixed with 3–5 mL/min N_2 to reduce BaO^+ formation (Miyazaki et al., 2014). Analyses were performed in static mode by simultaneously monitoring baseline-corrected ion currents corresponding to m/z 131 (Xe; L3), 135 (Ba; L1), 136 (Xe, Ba, Ce; center cup), 137 (Ba; H1), 138 (Ba, Ce, La; H2), 139 (La; H3), and 140 (Ce; H4) for 30 integrations, each ~ 4.2 s in duration. (Detector baselines were measured by deflecting the ion beam and measuring intensities for 30 s prior to each analysis.) Data reduction was performed using the three-dimensional geometric interpretation of the double spike problem (Siebert et al., 2001) whereby 138/135, 137/135, and 136/135 correspond to the x-, y-, and z-axes, respectively. Sample isotopic composition was solved iteratively—with additional nested loops for isobaric corrections—and reported relative to the nearest four bracketing measurements of NIST standard reference material 3104a in the delta-notation:

$$\delta^{138}\text{Ba}_{\text{NIST}} (\text{‰}) = \left(\frac{{}^{138}\text{Ba}_{\text{sample}}}{{}^{134}\text{Ba}_{\text{NIST}}} - 1 \right) \times 1000 \quad (\text{Eqn. 1})$$

Text S3. Additional Sampling and Analytical Protocols for pBa and pAl

GN01

Large and small fraction ($> 51 \mu\text{m}$ & $1 - 51 \mu\text{m}$) particulate samples were collected via McLane Research in situ pumps (WTS-LV) during the GN01 section (following Cutter et al., 2014). This paper reported total pBa (the sum of both large and small fractions). Original data are available at BCO-DMO (Lam, 2020). Pump casts were set up as described in Xiang & Lam (2020). Briefly, filter holders on the McLane pumps were prepared for two flow paths (quartz fiber “QMA” and polyethersulfone “Supor” flow paths) with 142 mm-diameter filter holders. Each path housed a “pre-filter” (51

μm polyester mesh; Sefar 07-51/33). Following the prefilter, the “QMA” path had paired 1.0 μm quartz fiber filters (Whatman QMA) that had been pre-combusted at 450°C for 4 hours. The “Supor” path had paired 0.8 μm polyethersulfone (Pall Supor800) filters. At basin stations (GN01), dBa was collected from the clean rosette which conducted two casts with a total of 23 depths (one overlapping depth). Particulate samples were typically collected from two pump casts for a total of 16 depths; at three stations, three casts were conducted for a total of 24 depths. In comparing the dBa to pBa, sample depths are often not a match.

Particulate barium and aluminum concentrations were obtained via a refluxing digestion method (Cullen & Sherrell, 1999; Ohnemus et al., 2014; Planquette & Sherrell, 2012). Briefly, the filter was placed onto the wall of a 15 mL flat-bottom screw-cap Savillex vial to avoid immersion. The digestion includes a 4-h refluxing at 110 °C with an ultrapure (ARISTAR® or *Optima*TM grade) 50% HNO₃/10% HF (v/v) mixture and drying down of the acid mixture. By ICP-MS (Thermo Scientific Element XR) at the UCSC Plasma Analytical Facility, final pBa sample solutions were analyzed in low resolution in low resolution. Indium (1 ppb) was used as an internal standard for ICP-MS analysis.

GN02/3

Detailed description of sampling and analysis are presented in Li (2017). Briefly, samples of particulate trace elements were collected from GO-FLO Bottles mounted on a trace metal clean rosette system. At all five stations, samples were collected between between 10 m and near bottom depth. Upon recovery, ~10 L of seawater were collected into LDPE cubitainers and was then filtered through a 0.45 μm Supor filter (47 mm diameter). The filters were subsequently dried, folded in half, and stored in clean poly bags until further analysis. Spaces, containers, and apparatuses were cleaned according to GEOTRACES protocols (Cutter et al., 2014).

Digestion of the particle samples was conducted at the University of British Columbia in a HEPA-filtered fume hood within a class 100 cleanroom. Filters were digested following the Piranha method (Ohnemus et al., 2014). Filters were placed in 15 mL Teflon vials (Savillex) and digested using a mixture of concentrated H₂SO₄ and concentrated H₂O₂ (1.2 mL and 0.4 mL, respectively) at high heat, to digest organic matter and filter matrix. For total digestion, 0.4 mL of concentrated H₂O₂ was added five times with a two hour reflux and slight drying between additions. Following refluxing, samples were dried, washed with 0.1 mL of 8N HNO₃, and dried again. The remaining materials were digested using a concentrated acid mixture of HNO₃:HCl:HF (i.e., 453 μL H₂O, 506 μL HNO₃, 687 μL HCl and 354 μL HF) at 110°C for 4 h. After complete drying, 1 mL of concentrated HNO₃ and 1 mL of concentrated H₂O₂ were added to the vials and taken to dryness again. Following this step, if the digest was yellow, which was uncommon, remaining organic matter was suspected,

and another 1 mL of concentrated HNO₃ and 1 mL of concentrated H₂O₂ were added, refluxed, and dried. To the ideal pellet, 0.1 mL of concentrated HNO₃ was added and taken to dryness.

For analysis by ICP-MS (Element2, Thermo Scientific), the final digest was re-suspended in 1% HNO₃ with 10 ppb Indium, as an internal standard. Instrumental blanks were monitored every 6 samples by measuring 1% HNO₃ with Indium. Detection limits and blanks are reported in Li (2017).

GN04

Suspended particles were sampled from the Dutch “ultraclean CTD” sampling system, Titan (de Baar et al., 2008), which consisted of 24 ultra-trace-metal clean polypropylene samplers of 24L each mounted on an all titanium frame with a SEABIRD 911 CTD system and deployed on a 11 mm Dyneema cable. After recovery, the complete “ultraclean CTD” was immediately placed in an ISO Class 6 clean room container, where samples for particulate trace elements were collected on 25mm diameter 0.45 µm polyethersulfone filters (Pall Supor) mounted in swinnex filter holders under pressure of filtered N₂ (0.7 bar) applied via the top-connector of the polypropylene sampler. Between 4 and 10L were filtered through the filters.

Particulate barium and aluminum concentrations were obtained via a refluxing digestion method (Planquette & Sherrell, 2012). Briefly, the filter was placed onto the wall of a 15 mL flat-bottom screw-cap Savillex vial to avoid immersion. The digestion includes a 4-h refluxing at 110 °C with an ultrapure (Merck) 50% HNO₃/10% HF (v/v) mixture and drying down of the acid mixture. Residues were re-dissolved using a 3% HNO₃ (v/v) solution then analyzed by SF-ICP-MS (Thermo Scientific Element XR) at the Pôle Spectrometrie Océans (France) in low resolution. Indium (1 ppb) was used as a drift monitor.

Text S5. Intercalibration of GEOTRACES Crossover Stations

The suite of cruises was conducted such that crossover stations, whereby two cruises occupied the same station, could occur (Figure S1). We report the locations of each crossover station in Table S2. Generally, the stations compare well and there are acceptably low offsets (Figure S2a). For dissolved Ba, calibration offsets > 2.5 are only observed in the upper 500 m of the water column where there is the influence of a strong halocline. Thus, in the upper 500 m of the water column small differences in depth may result in large changes in dBa. Similarly to dBa, pBa may also be influenced by the halocline and pBa offsets > 50 pM are only observed in the upper 500 m of the water column.

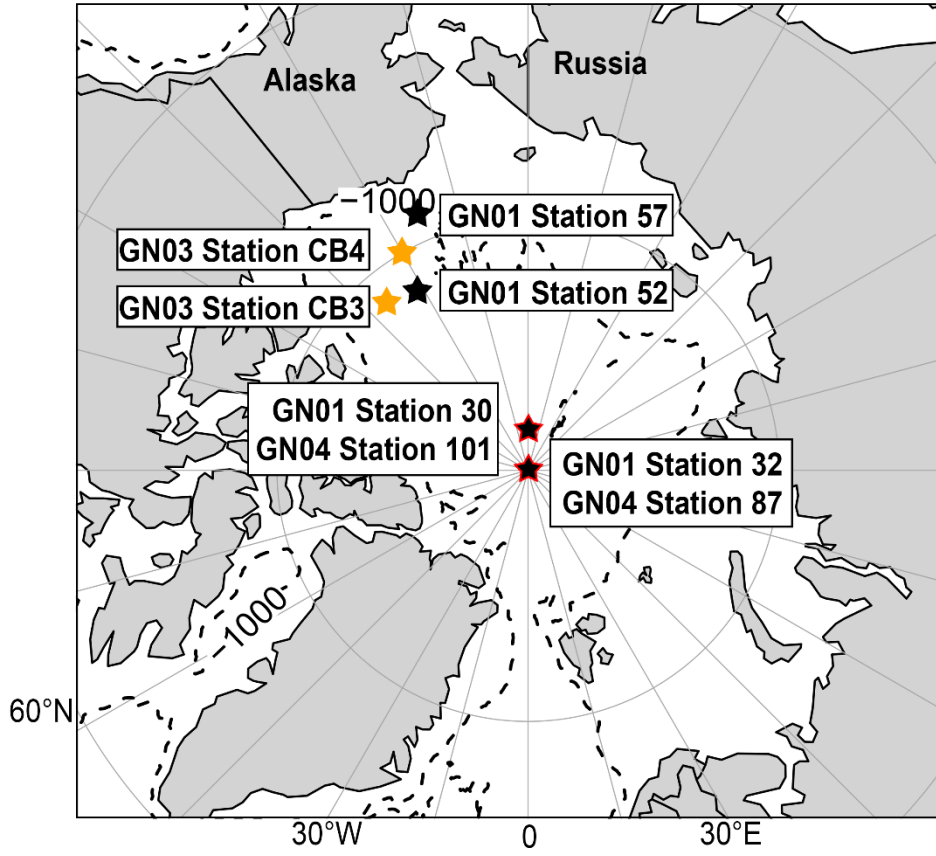


Figure S2. Cross-over station conducted in three separate 2015 Arctic GEOTRACES cruises. Black colors indicate US stations, red colors indicate European stations, and orange indicates Canadian stations.

Table S2. Intercalibration exercise between cruises.

Cruise	Station	Latitude (°N)	Longitude (°E)	Approximate Distance between stations (km)	Dissolved Ba (nmol kg ⁻¹)			Particulate Ba (pmol L ⁻¹)		
					Median Offset	Min Offset	Max Offset	Median Offset	Min Offset	Max Offset
GN01	32	89.99	32.54	7	0.63	0.24	1.84	49.2	21.5	96.9
GN04	87	89.93	-120.19							
GN01	30	87.52	-179.81	3	2.01	0.20	8.10	19.2	0.6	188.1
GN04	101	87.50	179.80							
GN01	57	73.39	-156.53	266	1.94	0.12	18.07	33.8	13.8	82.6
GN02/3	CB4	75.00	-150.00							
GN01	52	77.50	-148.01	203	1.10	0.14	10.76	31.9	10.5	161.2
GN02/3	CB3	76.99	-140.05							
Summary					1.40	0.12	18.07	31.5	0.6	188.1

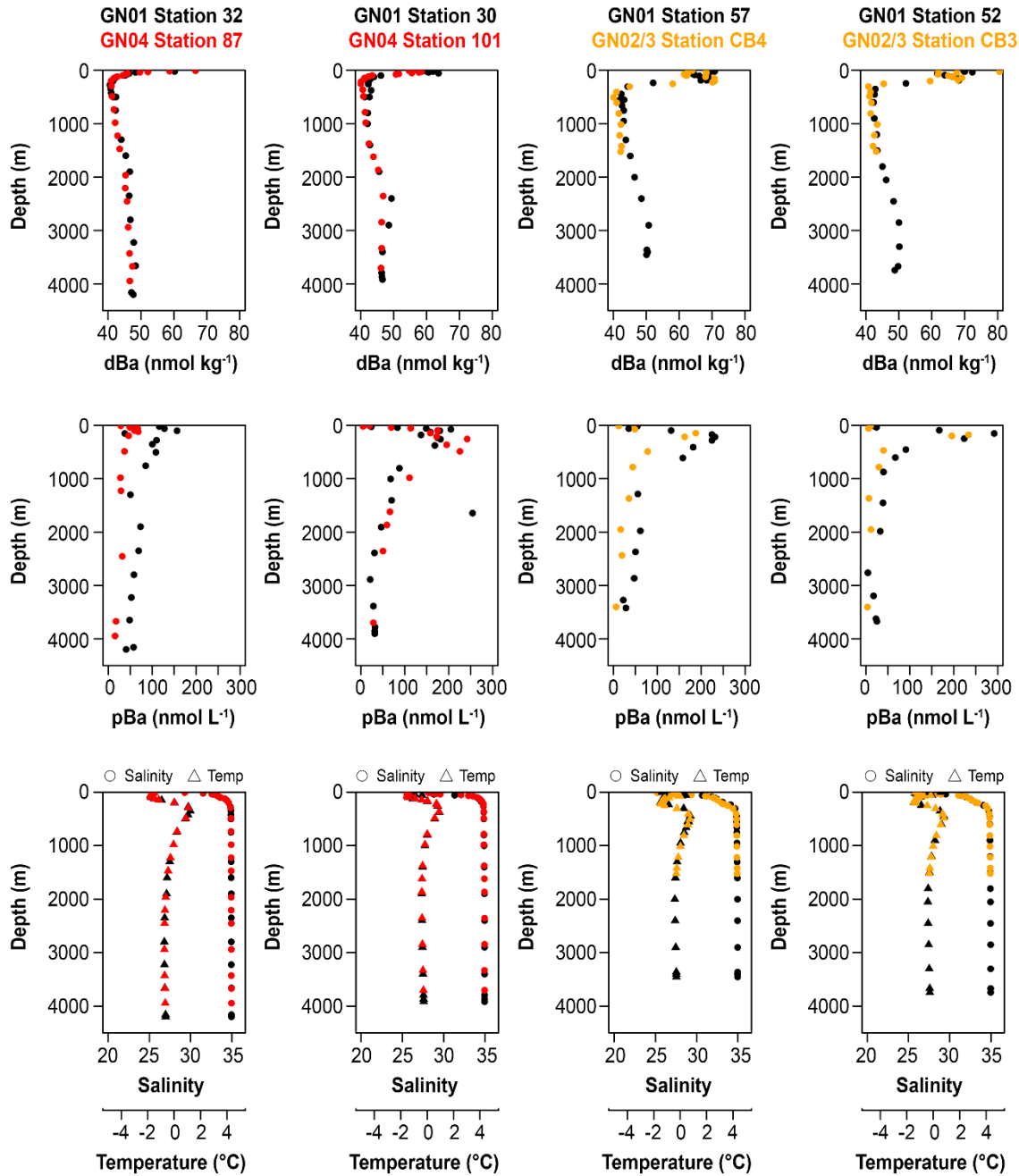


Figure S3. Cross-over station comparison. Following GEOTRACES Standards for intercalibration we compare for dBa (top row) and pBa (middle row) between stations conducted at roughly the same location on between cruises. The bottom row references temperature and salinity profiles for each station.

Text S6. Water Mass Deconvolution Approach

In this study we utilize a water mass deconvolution that leverage a linear endmember mixing model. In the upper 500 m of the Arctic Ocean we assign four

water types: Pacific-derived seawater (f_{pac}), Atlantic-derived seawater (f_{atl}), meteoric water (f_{met} ; river discharge and precipitation), and sea ice melt and formation (f_{ice}). Simply, to solve for the fraction of each water type (Eqn 1), we employ a series of tracer equations (Eqn 2 – 4) which are solved through an inverse matrix. Due to errors in laboratory analysis and the estimates of endmember concentrations, it is expected that fractions ($f_{parameter}$) will sometimes be negative, or greater than 1. Such excursions should be small, on the order of the reported errors. Highly negative values of f_{pac} , f_{atl} , or f_{met} are indicative of a larger issue, such as poor endmember selection).

$$\text{Eqn 1.} \quad f_{pac} + f_{atl} + f_{met} + f_{ice} = 1$$

$$\text{Eqn 2.} \quad S_{pac} \cdot f_{pac} + S_{atl} \cdot f_{atl} + S_{met} \cdot f_{met} + S_{ice} \cdot f_{ice} = S_{obs}$$

$$\text{Eqn 3.} \quad O_{pac} \cdot f_{pac} + O_{atl} \cdot f_{atl} + O_{met} \cdot f_{met} + O_{ice} \cdot f_{ice} = O_{obs}$$

$$\text{Eqn 4.} \quad N_{pac} \cdot f_{pac} + N_{atl} \cdot f_{atl} + N_{met} \cdot f_{met} + N_{ice} \cdot f_{ice} = N_{obs}$$

Because there are four unknowns in Eqn. 1, we require three tracers to deconvolve constrain the system. We employ salinity (S), the stable isotope (^{18}O) of water, and a nutrient tracer (N). The nutrient tracer relies on a predictable difference in the N:P ratio between Atlantic and Pacific Seawater (Newton et al., 2013). The endmembers of each tracer for each water type have been extensively considered in previous literature (e.g., Bauch et al., 2011; Newton et al., 2013; Whitmore et al., 2020) and are tabulated below. The uncertainties related with this approach are also well articulated in other literature (e.g., Alkire et al., 2015).

Table S3. Endmember values for water type tracers.

Water type	^a Salinity (S)	^a $\delta^{18}\text{O}$ [‰] (O)	^b Nutrient Tracer (N)
Pacific water	32.50 ± 0.20	-1.1 ± 0.20	1
Atlantic water	34.92 ± 0.03	0.3 ± 0.05	0
Meteoric water	0	-20 ± 2	0
Sea ice meltwater	4 ± 1	Surface + 2.6	Surface

^a Newton et al., 2013 and references therein.

^b Whitmore et al., 2020

In the distributions (Figure S4), we observed Pacific water predominantly expressed in the Amerasian Arctic Ocean basin. Meteoric water was predominantly expressed in the surface ocean, with the highest abundance in the Transpolar Drift. Sea ice melt signals were highest in the surface ocean near the ice edge. Brine signals were highest in the halocline and in transpolar drift waters.

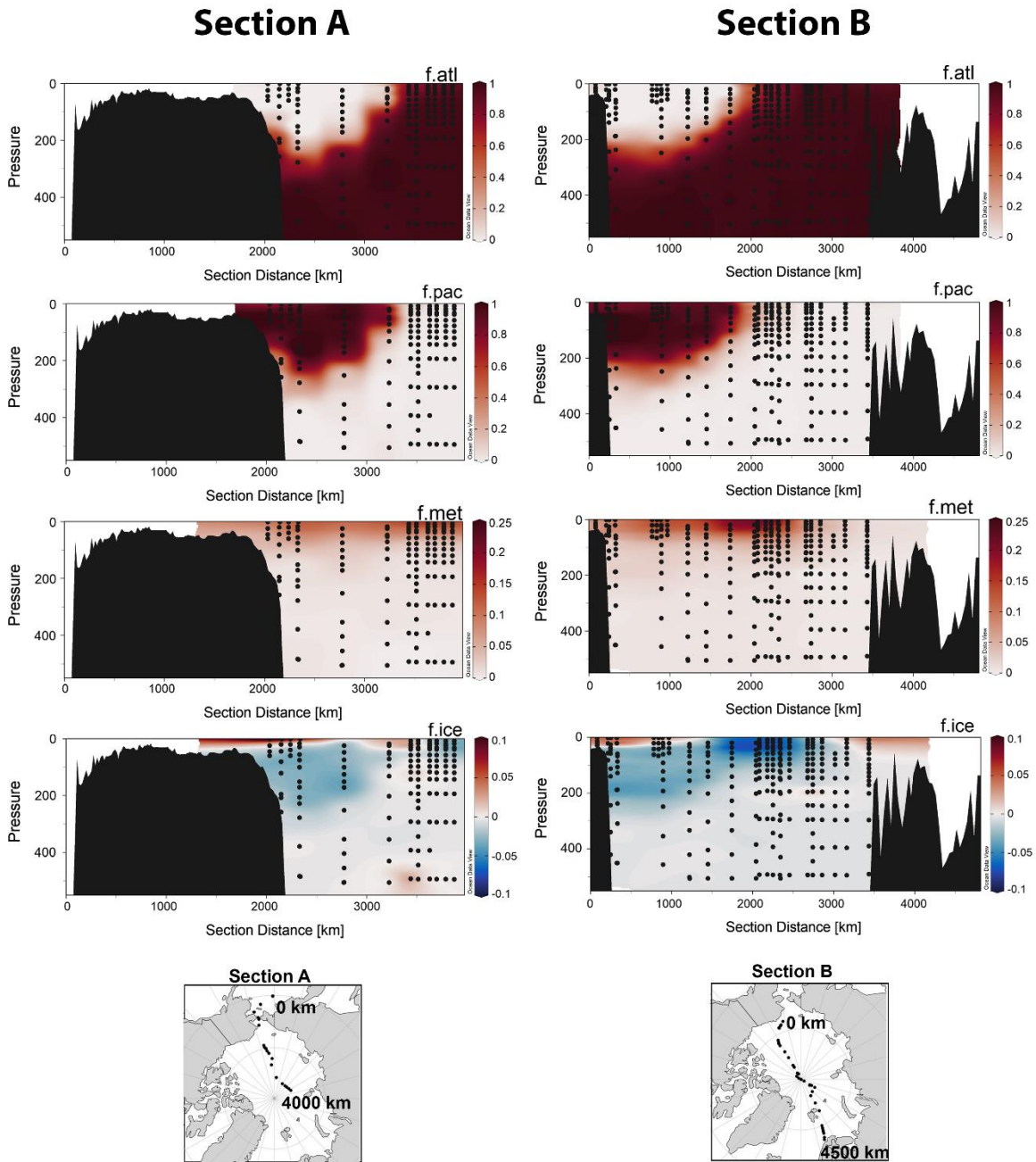


Figure S4. Distributions of water mass fractions in Sections A and B.

Text S7. Discussion on Sensitivity

We, in all our models, perturbed the endmembers by 15% to see what parameters the models are most sensitive to. We further assessed the variability in our results by determining the maximum, minimum, and “best estimate” dBa_{pred} using the ranges of dBa endmembers (Section 3.2.1; Table 1), such that we assessed maximum and minimum values for all endmembers at once (the most extreme plausible conditions).

The first model herein is the predicted Ba distribution (dBa_{pred}) which relies on the fraction of each water mass determined as described in Text S4. We consider sensitivity in the dBa_{pred} (and $\text{Ba}_{\text{anomaly}}$) first. See Section 3.2 of the manuscript for equations of these parameters or Section 5.1 for discussion of the results. dBa_{pred} (Section 3.2 and 5.1) and determined that – for a 15% perturbation - results were most sensitive to perturbation in the Atlantic endmember values: +9.9% increase in dBa_{pred} versus a +1.6%, +3.4%, and 0% increases for perturbations in meteoric, Pacific, and sea ice endmembers, respectively. Using these sensitivity analyses we conclude that dBa_{pred} is insensitive to a 15% change in sea ice endmember concentration. There is less than 10% uncertainty with respect to error associated with endmember selection. By propagating uncertainties of dBa_{pred} and dBa_{obs} we estimate that $\text{Ba}_{\text{anomaly}}$ has an uncertainty $\sim 11\%$ (generally around 5 nmol kg^{-1}).

We used violin plots to demonstrate how distributions of data change under different conditions (Figure S5). The first condition presented is the case in which the endmembers or fractions are perturbed by 15% (Figure S5 a-b); the second condition is the case in which the endmember ranges are most important in setting the distributions. This case includes an extra case (“Sea Ice High”) whereby the endmembers used are the same as for the maximum case except the maximum Sea Ice is increased to 60 nM. We note that the case for the *maximum* and the *Sea Ice High* conditions are effectively the same as the maximum condition, indicating little effect of an increased Sea Ice endmember (Figure S5 c-d).

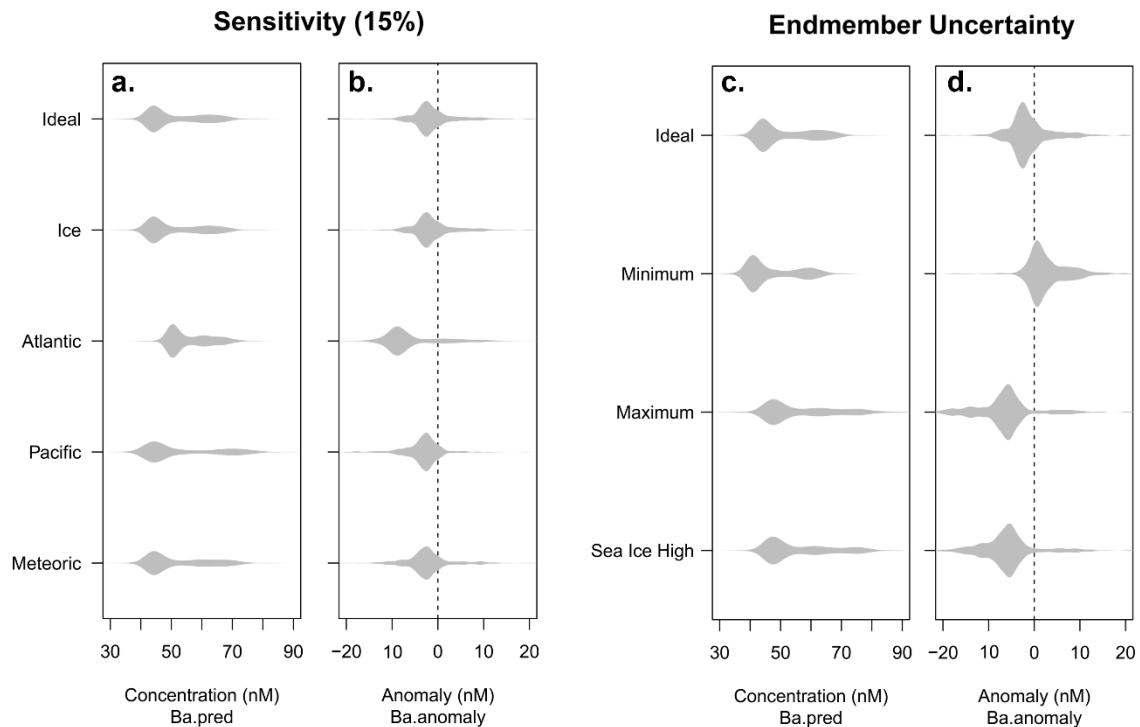


Figure S5. Violin plots showing the distribution of $\text{Ba}_{\text{predicted}}$ and $\text{Ba}_{\text{anomaly}}$ data under

various perturbations. The models are most sensitive to the Atlantic endmember/fraction.

In considering sensitivity of the barium isotope model (Section 5.2), the parameters that must be considered are the isotope endmember (predicted as a result), the concentration endmember (predetermined) and the fraction of each water type (predetermined). The endmember concentrations and fractions have the same uncertainties as described for $Ba_{\text{predicted}}$. The effect of these uncertainties on predicted $\delta^{138}\text{Ba}$ was negligible for the Atlantic and Pacific endmembers (regardless of whether ice is included in the model; Table S4). The meteoric endmember prediction ranges between 0.30 and 0.35 (up to 15% variance), which is nearly within uncertainty of the measurements and is well within the predicted meteoric isotope range. We note also that optimizations may be influenced by the initial parameters, and we have run the model under randomized initial parameters with no effect on the endmember predictions (data not shown). Thus, variation in the endmembers and initial parameter values does not influence our interpretation of the results.

Table S4. Sensitivity of predicted $\delta^{138}\text{Ba}$ endmembers.

	Endmember Conditions				Predicted $\delta^{138}\text{Ba}$ Endmember			
	Meteoric	Atlantic	Pacific	Sea Ice	Meteoric	Atlantic	Pacific	Sea Ice
Best Guess	130	42	56	6.5	0.32	0.57	0.36	1.12
	130	42	56		0.33	0.57	0.36	
Minimum	90	39	55	2	0.30	0.57	0.37	2.21
	90	39	55		0.31	0.57	0.36	
Maximum	190	45	57	11	0.34	0.57	0.36	0.99
	190	45	57		0.35	0.57	0.36	
Sea Ice High	190	45	57	60	0.34	0.56	0.37	0.53
	190	45	57		0.35	0.57	0.36	

We also consider sensitivity of the box model (Section 5.4). In perturbing the endmembers by 15% we reveal that the system is most sensitive to the Ba inventory and residence time components, followed by Atlantic components (concentration or flux). Perturbations (by 15%) in the inventory and the residence time resulted in a ~35% and ~30% change in the net nonconservative flux, respectively. The model was insensitive to river and Pacific concentration or flux (Figure S6). In the manuscript we present a range of likely mass balance results by considering the potential range in endmember concentrations. We've chosen these endmember concentrations considering several aspects of the environmental system and model (discussed in section 3.2.1 of the manuscript). Here, we articulate that the budget cannot be closed by increasing the river endmember to any observed river concentration (i.e., 500 nM, Mackenzie River discharge). By using the Barents Sea volume flux (rather than the Fram Strait volume flux with standard deviation) we demonstrate that the budget can become effectively closed (80% resolved). We note also, perturbing the residence time, as demonstrated in the sensitivity analysis has the greatest potential

to close the budget. An increase to a 20-year residence time fully closes the budget under ideal conditions. An increase to 15 years, the approximate residence time of the halocline, results in a budget that is 78% resolved.

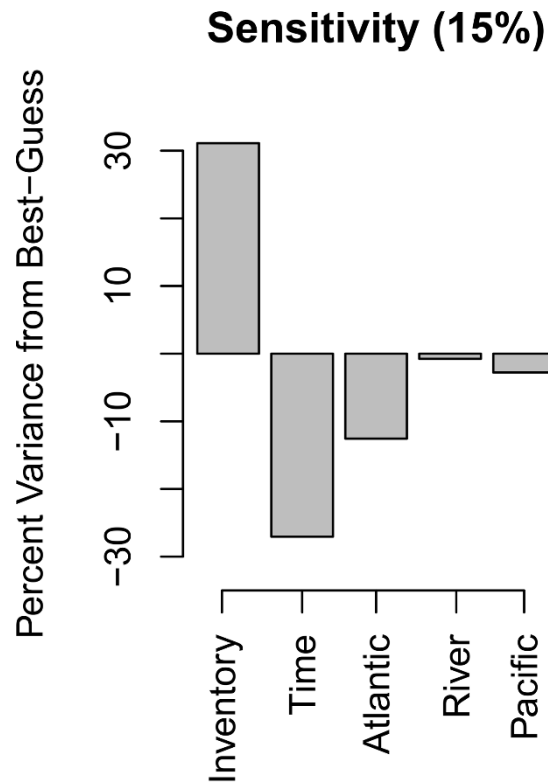


Figure S6. Sensitivity of the box model to a 15% perturbation on individual parameters in the model.

Text S8. Comparison of dBa and pBa to the North Pacific and North Atlantic Oceans

The distribution of dissolved and particulate Ba in the western Arctic Ocean is unique compared to vertical distributions in the North Pacific and North Atlantic Oceans (Figure S7). Dissolved Ba distributions in the North Pacific and Atlantic follow a nutrient-like profile shape: low in the surface and generally increasing with depth. In the western Arctic Ocean basins, dBa is highest in the surface waters (< 300 m) and decreases between 300 and 2000 m depth before increasing toward the bottom.

Particulate Ba usually has a mesopelagic maximum; in the western Arctic Ocean the maximum is slightly shallower than in other ocean basins.

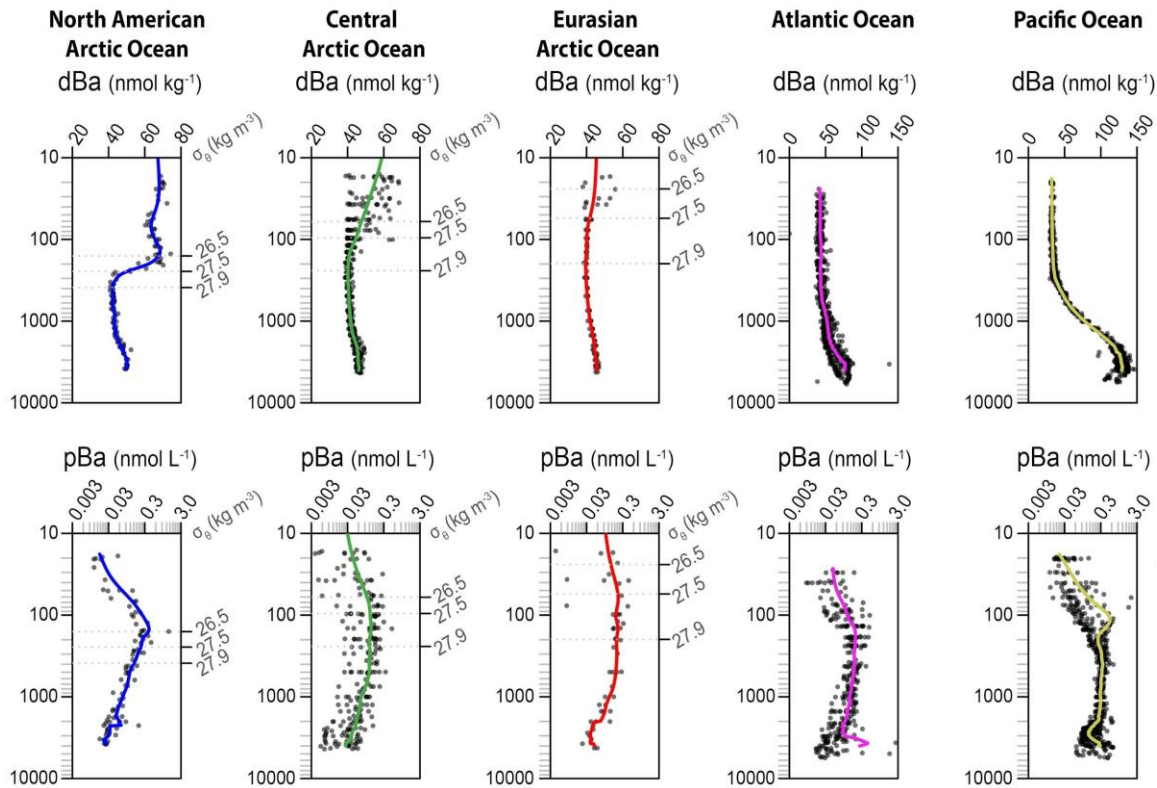


Figure S7. Comparison of Arctic Ocean dBa and pBa vertical distributions to the Pacific Ocean (GP16) and Atlantic Ocean (GA03). Data for the Atlantic and Pacific Oceans was extracted from the GEOTRACES Intermediate Data Product (Version 2) (Schlitzer et al., 2018).

Text S9. The Flux Balance Approach to the dissolved Ba Budget

The box we consider in our elemental budget is the upper 500 m of the Arctic Ocean water column where bottom depths are greater than 1000 m (Figure S8). Two datasets are used separately to consider how the balance has changed since the early measurements of dBa in the Arctic Ocean: the 2015 Arctic GEOTRACES data and the 1994 Arctic Ocean Survey.

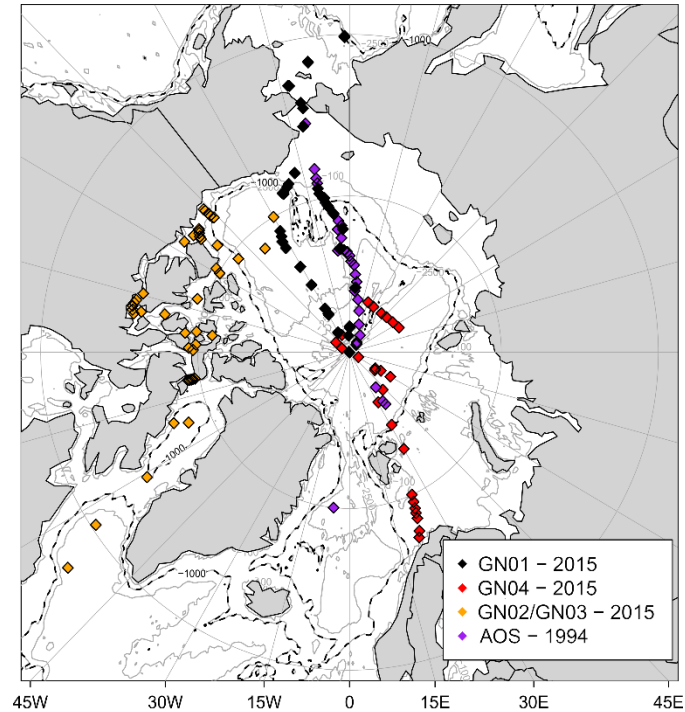


Figure S8. The spatial outer bounds of the box model are roughly identified in this figure. The 1000 m isobath is identified by the dashed line, the model is informed by all data points north of the Bering Strait, Fram Strait, and Canadian Arctic Archipelago (i.e., the Arctic Ocean Basins). Two scenarios were run using data from the 2015 GEOTRACES surveys and from the 1994 AOS survey.

Text S10. Comparison of the box model results to Ra-flux predicted Ba fluxes

In the manuscript text we described the results of our box model, which indicated that approximately 50% of the Ba budget in the basins is sourced from the shelves. As a secondary assessment to the box model predicted fluxes, we used the $dBa:^{228}Ra$ relationship on the shelf to predict the fluxes of dBa from shelf sediments such that: $F_{Ba} = \frac{dBa}{dRa} \times F_{Ra}$. Where F indicates flux (with the superscript representing the element) and dBa and dRa indicating the ratio of those elements on the shelves. The flux of radium (F_{Ra} in atoms/y) was directly from Kipp et al. (2018). We determined the dBa:dRa ratio using shelf dBa (nmol/L) data from this study and shelf ^{228}Ra data from Kipp et al. (2018). The ratio used is the regression of the two parameters (Figure S9).

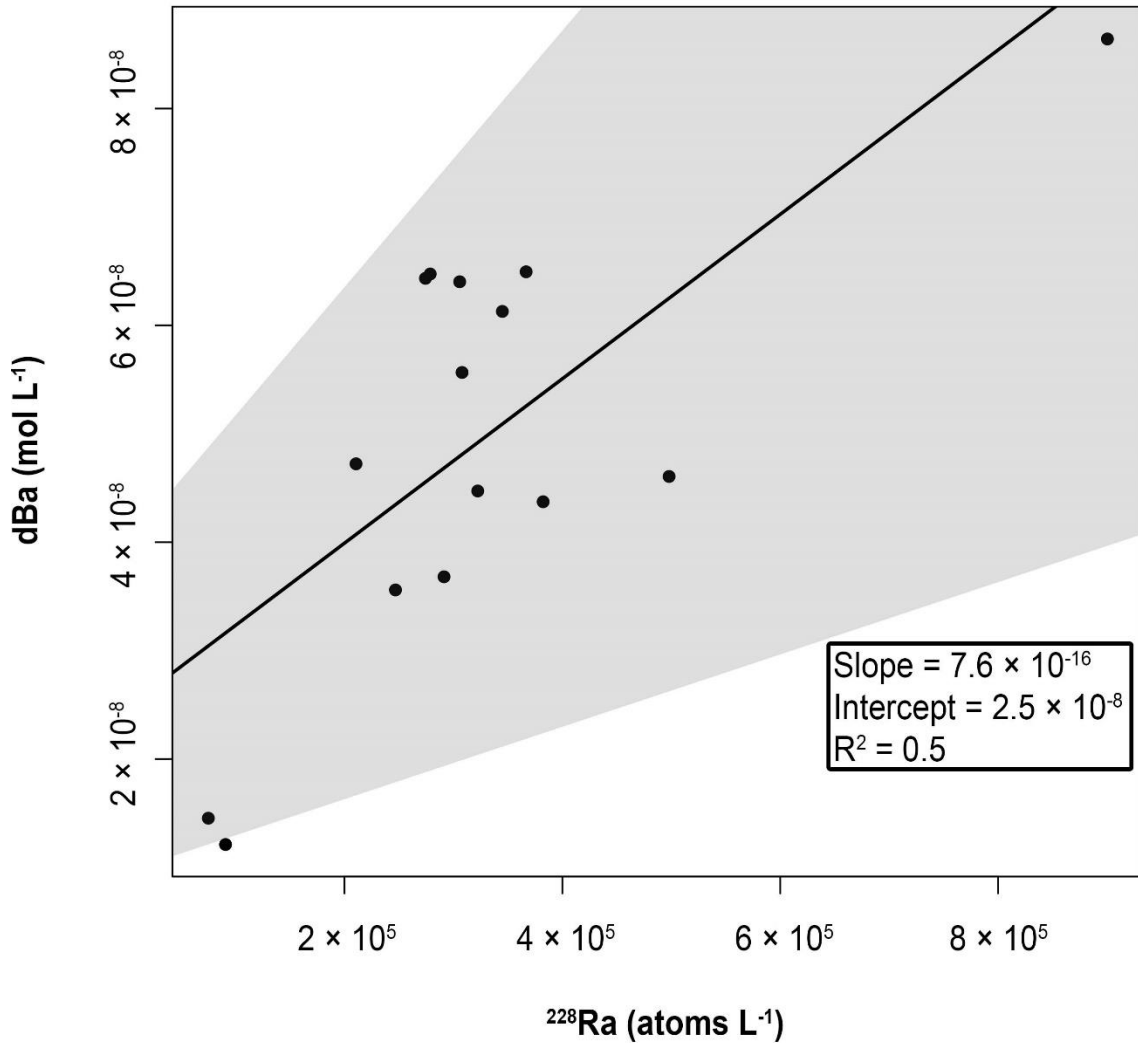


Figure S9. The observed relationship between dBa and dissolved ^{228}Ra . Data points are from the western Arctic shelves (Bering and Chukchi Sea) sampled during the 2015 GN01 expedition. The black line is a type II linear regression and the gray shaded area is the 95% confidence interval.

Text S11. Evidence of hydrothermal Ba in the Eurasian Arctic

Two stations in the GN04 transect sit near the Nansen-Gakkel Ridge Crest. One station has dissolved distributions of dBa that reflect hydrothermal input (i.e., deep water maxima between 2000 and 3000 m; Figure S10).

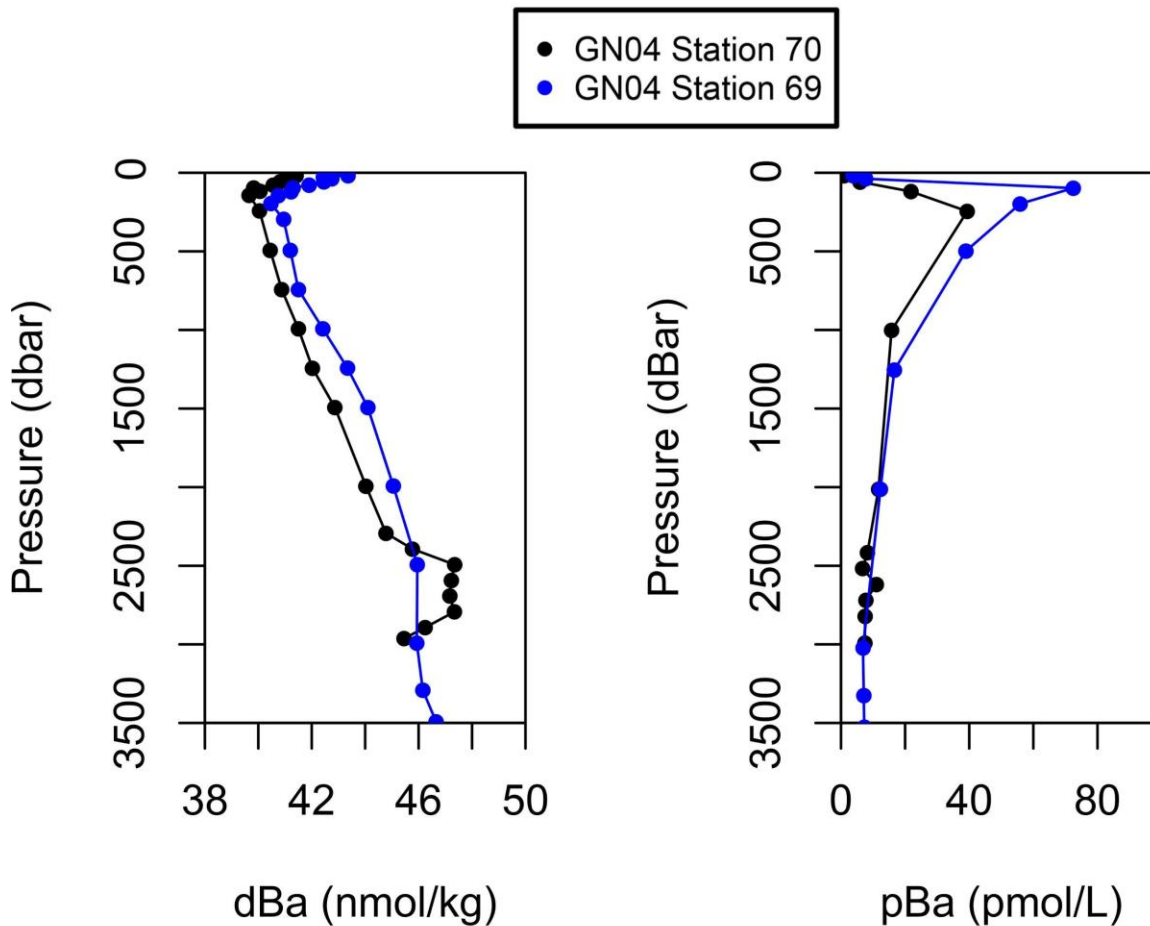


Figure S10. Nansen-Gakkel Ridge Crest Stations. The black dots and lines represent station 70, which appears to be influenced by a dBa source between 2000 and 3000 dbar (hydrothermal input); there also may be a slight input of pBa to the water column. Blue lines are the nearby station 69; which does not appear to be influenced by the hydrothermal plume.

Text S12. Dissolved Ba Salinity Relationships in the Canadian Arctic Archipelago

We investigated the dBa-Salinity relationships to probe how rivers or sea ice melt might influence dBa concentrations. Broadly through the Archipelago there are two salinity patterns. At high salinities ($S > 32.5$), dBa decreases with increasing S (Figure S11a). This is consistent with mixing of Atlantic-source water with Pacific-origin waters in the Arctic Ocean basins. However, we note that there is a large amount of scatter in the CAA trend, which is not observed in the Arctic Ocean. At low salinities ($S < 32.5$) dBa decreases slightly, which is roughly in line with how a slight contribution of sea ice would dilute the seawater concentrations. We suspect there is not a large river influence as at low salinities ($S < 32.5$) since dBa decreases; generally, rivers have high dBa signatures and would drive dBa up at low salinity. We

note that the concentrations of dBa in CAA rivers is not well constrained, but studies show a broad range of possible endmember (Colombo et al., 2019). Most of the possible endmembers are higher than seawater, but a few do fall below the seawater concentration. Thus, it is possible there is slight river influence in addition to sea ice melt at the low salinity range.

Here, we diagnose the reason for the scatter at the high salinity range by looking at stations in the CAA (Parry Channel) moving from the Arctic Ocean eastward to Lancaster Sound (Figure S11b-d). We follow the dBa at each station and highlight the dBa at $S = 32.5$, the salinity of Pacific-derived seawater. Moving eastward, dBa at $S = 32.5$ decreases, furthermore, the dBa on the north side of the channel (CAA4 and CAA6) can be substantially lower than on the south side of the channel (CAA5 and CAA7). We note that CAA7 is tucked just south of the Parry Channel, in a northward flowing channel of the Archipelago. Due to its position, it may not be perfectly representative of waters flowing from the Arctic through Parry Channel. On the south side of the Parry Channel, dBa decreased to ~ 56 nmol/kg at $S = 32.5$ (from ~ 65 nmol/kg in the Canada Basin and western extent of Parry channel). On the north side of the channel, dBa reached as low as 50 nmol/kg at $S = 32.5$. We suggest this erosion of the high dBa signal is due to mixing of Atlantic-like waters in Baffin Bay with the eastern extent of the Parry Channel.

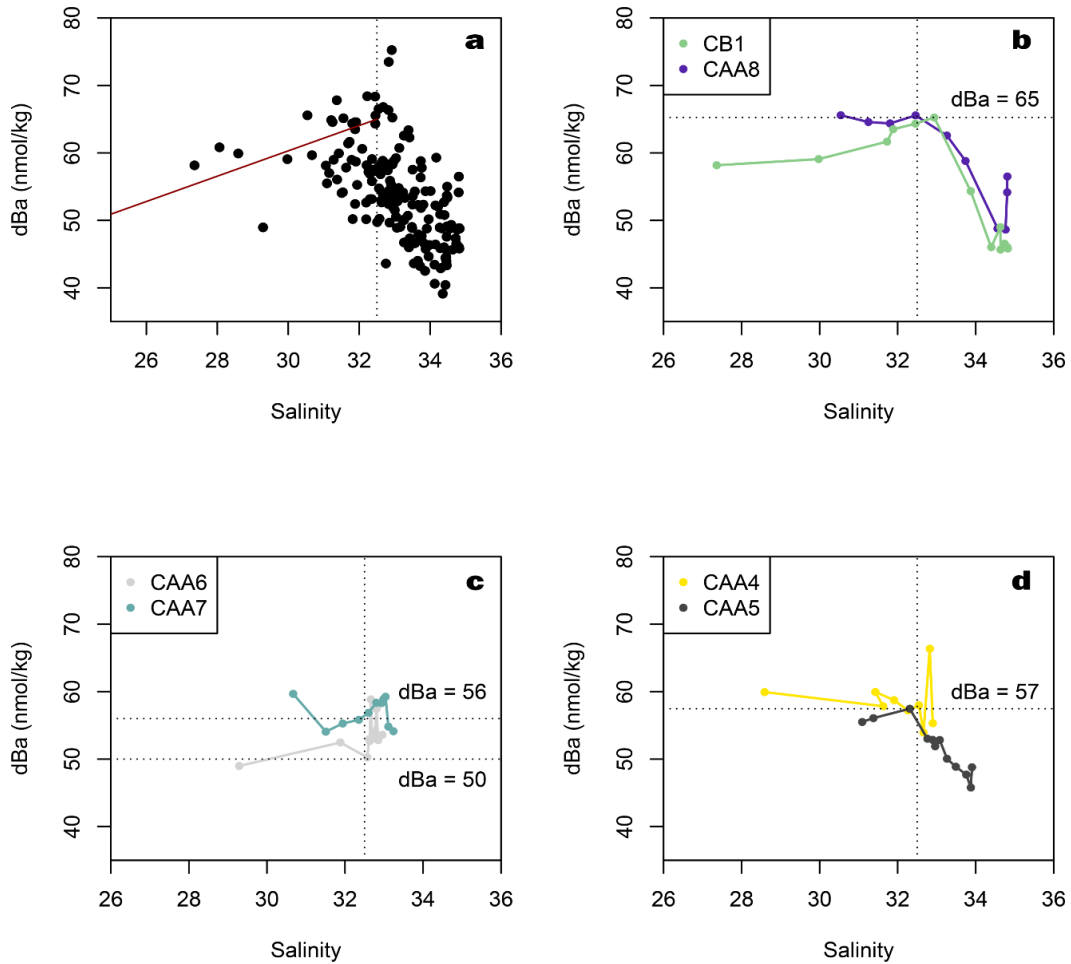


Figure S11. dBa-Salinity patterns in the CAA. In all panels the dashed vertical line is $S = 32.5$ and is representative of Pacific-derived seawater; the dashed horizontal line is the dBa at $S = 32.5$. a) all stations and samples in the Parry Channel. The red line denotes mixing with sea ice melt. b) Stations on the Arctic Ocean (western) side of the Parry Channel; CB1 is in the Canada Basin and CAA8 is in the Parry Channel. Both of these stations have a “western Arctic Ocean-like” signal, where Pacific-derived seawater is high in dBa (~65 nmol/kg). c) Stations CAA6 and CAA7 (just west of the Barrow Strait in Parry Channel). Dissolved Ba has decreased to 56 nmol/kg on the south side of the Channel and 50 nmol/kg on the north side of the channel. d) Stations CAA4 (north side of channel) and CAA5 (south side of channel) are located just east of the Barrow Strait. They have roughly equivalent dBa (57 nmol/kg).

References

- Bauch, D., van der Loeff, M. R., Andersen, N., Torres-Valdes, S., Bakker, K., & Abrahamsen, E. P. (2011). Origin of freshwater and polynya water in the Arctic Ocean halocline in summer 2007. *Progress in Oceanography*, 91(4), 482–495. <https://doi.org/10.1016/j.pocean.2011.07.017>
- Colombo, M., Brown, K. A., De Vera, J., Bergquist, B. A., & Orians, K. J. (2019). Trace metal geochemistry of remote rivers in the Canadian Arctic Archipelago. *Chemical Geology*, 525, 479–491. <https://doi.org/10.1016/j.chemgeo.2019.08.006>
- Cullen, J. T., & Sherrell, R. M. (1999). Techniques for determination of trace metals in small samples of size-fractionated particulate matter: phytoplankton metals off central California. *Marine Chemistry*, 67(3–4), 233–247. [https://doi.org/10.1016/S0304-4203\(99\)00060-2](https://doi.org/10.1016/S0304-4203(99)00060-2)
- Cutter, G., Andersson, P. S., Codispoti, L. A., Croot, P., Francois, R., Lohan, M., et al. (2014). Sampling and Sample-handling Protocols for GEOTRACES Cruises, Version 2. <http://www.geotraces.org/library-88/scientific-publications/reports/169-sampling-and-sample-handling-protocols-for-geotraces-cruises>
- De Baar, H. J. W., Timmermans, K. R., Laan, P., De Porto, H. H., Ober, S., Blom, J. J., et al. (2008). Titan: A new facility for ultraclean sampling of trace elements and isotopes in the deep oceans in the international Geotraces program. *Marine Chemistry*, 111(1–2), 4–21. <https://doi.org/10.1016/j.marchem.2007.07.009>
- Fetterer, F., Knowles, K., Meier, W., Savoie, M., & Windnagel, A. (2017). Sea Ice Index, Version 3 [Data set]. NSIDC. <https://doi.org/10.7265/N5K072F8>
- Kipp, L. E., Charette, M. A., Moore, W. S., Henderson, P. B., & Rigor, I. G. (2018). Increased fluxes of shelf-derived materials to the central Arctic Ocean. *Science Advances*, 4(1), eaao1302. <https://doi.org/10.1126/sciadv.aao1302>
- Klinkenberg, H., Van Borm, W., & Souren, F. (1996). A theoretical adaptation of the classical isotope dilution technique for practical routine analytical determinations by means of inductively coupled plasma mass spectrometry. *Spectrochimica Acta Part B: Atomic Spectroscopy*, 51(1), 139–153. [https://doi.org/10.1016/0584-8547\(95\)01386-5](https://doi.org/10.1016/0584-8547(95)01386-5)
- Klinkhammer, G. P., & Chan, L. H. (1990). Determination of barium in marine waters by isotope dilution inductively coupled plasma mass spectrometry. *Analytica Chimica Acta*, 232, 323–329.
- Lam, P. (2020). Size-fractionated major and minor particle composition and concentration from the US GEOTRACES Arctic cruise (HLY1502) on USCGC Healy from August to October 2015. (Version (Version 1) Version Date 2020-04-01). Biological and Chemical Oceanographic Data Management Office (BCO-DMO).
- Li, J. (2017). *Particulate Trace Metals & Iron Availability to Phytoplankton in a Changing Arctic Ocean* (Masters of Science). University of British Columbia.

- Miyazaki, T., Kimura, J.-I., & Chang, Q. (2014). Analysis of stable isotope ratios of Ba by double-spike standard-sample bracketing using multiple-collector inductively coupled plasma mass spectrometry. *Journal of Analytical Atomic Spectrometry*, 29(3), 483. <https://doi.org/10.1039/c3ja50311a>
- Newton, R., Schlosser, P., Mortlock, R., Swift, J., & MacDonald, R. (2013). Canadian Basin freshwater sources and changes: Results from the 2005 Arctic Ocean Section: AOS 2005 freshwater sources and changes. *Journal of Geophysical Research: Oceans*, 118(4), 2133–2154. <https://doi.org/10.1002/jgrc.20101>
- Ohnemus, D. C., Auro, M. E., Sherrell, R. M., Lagerström, M., Morton, P. L., Twining, B. S., et al. (2014). Laboratory intercomparison of marine particulate digestions including Piranha: a novel chemical method for dissolution of polyethersulfone filters. *Limnology and Oceanography: Methods*, 12(8), 530–547. <https://doi.org/10.4319/lom.2014.12.530>
- Planquette, H., & Sherrell, R. M. (2012). Sampling for particulate trace element determination using water sampling bottles: methodology and comparison to in situ pumps: Particulate trace element sampling. *Limnology and Oceanography: Methods*, 10(5), 367–388. <https://doi.org/10.4319/lom.2012.10.367>
- Schlitzer, R., Anderson, R. F., & Masferrer Dodas, E. (2018). The GEOTRACES Intermediate Data Product 2017. *Chemical Geology*. <https://doi.org/10.1016/j.CHEMGEO.2018.05.040>
- Siebert, C., Nögler, T. F., & Kramers, J. D. (2001). Determination of molybdenum isotope fractionation by double-spike multicollector inductively coupled plasma mass spectrometry. *Geochemistry, Geophysics, Geosystems*, 2(7), 2000GC00124. <https://doi.org/10.1029/2000GC000124>
- Webster, R. K. (1960). Mass spectrometric isotope dilution analysis. In *Methods in geochemistry* (pp. 202–246). London: Interscience.
- Whitmore, L. M., Pasqualini, A., Newton, R., & Shiller, A. M. (2020). Gallium: A New Tracer of Pacific Water in the Arctic Ocean. *Journal of Geophysical Research: Oceans*, 125(7). <https://doi.org/10.1029/2019JC015842>
- Xiang, Y., & Lam, P. J. (2020). Size-fractionated marine suspended particle dynamics in the Western Arctic Ocean: Lateral and vertical sources. *Journal of Geophysical Research: Oceans*, 125(8), e2020JC016144.